Earth's Future

RESEARCH ARTICLE
10.1029/2025EF006918

Detectability of Post-Net Zero Climate Changes and the Effects of Delay in Emissions Cessation

Andrew D. King[1,2], Eduardo Alastrué de Asenjo[3,4], Amanda C. Maycock[5], Tilo Ziehn[6], Alexander R. Borowiak[2], Spencer Clark[1,2], and Nicola Maher[1,7]

[1]ARC Centre of Excellence for 21st Century Weather, Clayton, VIC, Australia, [2]School of Geography, Earth and Atmospheric Sciences, University of Melbourne, Melbourne, VIC, Australia, [3]Institute of Oceanography, Center for Earth System Research and Sustainability (CEN), University of Hamburg, Hamburg, Germany, [4]Max Planck Institute for Meteorology, Hamburg, Germany, [5]School of Earth and Environment, University of Leeds, Leeds, UK, [6]CSIRO Environment, Aspendale, VIC, Australia, [7]Research School of Earth Sciences, The Australian National University, Canberra, ACT, Australia

Key Points:

- We examine detectability of global, regional and local climate change measures using millennial-scale net zero CO_2 emissions simulations
- Detectable changes under net zero are found in temperature and precipitation means and extremes, Atlantic Meridional Overturning Circulation recovery, and sea ice extent
- Delays to emissions cessation have widespread consequences for many centuries

Supporting Information:

Supporting Information may be found in the online version of this article.

Correspondence to:

A. D. King,
andrew.king@unimelb.edu.au

Citation:

King, A. D., Alastrué de Asenjo, E., Maycock, A. C., Ziehn, T., Borowiak, A. R., Clark, S., & Maher, N. (2025). Detectability of post-net zero climate changes and the effects of delay in emissions cessation. *Earth's Future*, *13*, e2025EF006918. https://doi.org/10.1029/2025EF006918

Received 13 JUL 2025
Accepted 30 SEP 2025

Author Contributions:

Conceptualization: Andrew D. King
Data curation: Andrew D. King, Eduardo Alastrué de Asenjo, Tilo Ziehn
Formal analysis: Andrew D. King
Methodology: Andrew D. King
Visualization: Andrew D. King
Writing – original draft: Andrew D. King
Writing – review & editing: Andrew D. King, Eduardo Alastrué de Asenjo, Amanda C. Maycock, Tilo Ziehn, Alexander R. Borowiak, Spencer Clark, Nicola Maher

Abstract There is growing interest in how the climate would change under net zero carbon dioxide emissions pathways as many nations aim to reach net zero in coming decades. In today's rapidly warming world, many changes in the climate are detectable, even in the presence of internal variability, but whether climate changes under net zero are expected to be detectable is less well understood. Here, we use a set of 1000-year-long net zero carbon dioxide emissions simulations branching from different points in the 21st century to examine detectability of large-scale, regional and local climate changes as time passes under net zero emissions. We find that even after net zero, there are continued detectable changes to climate for centuries. While local changes and changes in extremes are more challenging to detect, Southern Hemisphere warming and Northern Hemisphere cooling become detectable at many locations within a few centuries under net zero emissions. We also study how detectable delays in achieving emissions cessation are across climate indices. We find that for global mean surface temperature and other large-scale indices, such as Antarctic and Arctic sea ice extent, the effects of an additional 5 years of high greenhouse gas emissions are detectable. Such delays in emissions cessation result in significantly different local temperatures for most of the planet, and most of the global population. The long simulations used here help with identifying local climate change signals. Multi-model frameworks will be useful to examine confidence in these changes and improve understanding of post-net zero climate changes.

Plain Language Summary The rapid pace of climate change is observed in many aspects of the Earth system including local warming and rainfall changes, increases in some extremes, and decreasing ice in polar regions. These observable climate change effects have been part of the motivation for the Paris Agreement and the push to achieve net zero emissions. There is a growing understanding that we should expect some aspects of the climate to continue changing under net zero and that there are benefits to getting to net zero sooner, but it has been unclear to date whether these changes will be obvious or masked by noise in the climate. Here we use simulations to examine how apparent climate changes may be under net zero and the effects of delays in achieving net zero. We find that over time, detectable changes in the climate system still occur under net zero. Many people live in places where we identify detectable local climate changes under net zero emissions. Delays in getting to net zero have identifiable effects across many aspects of the climate system. Achieving net zero should not be expected to halt all climate changes, but it is a necessary step in reducing climate change impacts.

1. Introduction

The world is warming rapidly due to human activities. Global-mean surface temperatures are now more than 1.3°C above pre-industrial levels (Forster et al., 2025) and multiple observed global and regional climate changes have been robustly detected and attributed to human influence (Eyring et al., 2021). The rapidly changing climate and associated impacts have motivated nations to adopt net zero greenhouse gas emissions targets for the coming decades. By achieving net zero emissions, global warming may be halted, or at least substantially slowed down (Borowiak et al., 2024; MacDougall et al., 2020), and further climate change impacts may be limited. However, relatively little is known about the characteristics of a post-net zero climate compared to a warming climate.

While global temperature changes are likely to be small under net zero emissions, regional and local changes may still be substantial (Cassidy et al., 2023; MacDougall et al., 2022). It is important that such changes can be anticipated to manage societal expectations about where and when the benefits of mitigation will become evident.

A challenge for communicating the evidence for climate change, and in turn the benefits of mitigation, is the potential for internal climate variability to mask long-term changes over annual to decadal timescales. To date, the clearest emergence of changes in local temperatures and temperature extremes is over low-latitude regions (Hawkins et al., 2020; A. D. King et al., 2015; Mahlstein et al., 2012). In contrast, for precipitation and extreme precipitation, the changes are less distinguishable from natural variability, and emergence is slightly clearer over northern high latitudes than elsewhere (Hawkins et al., 2020; A. D. King et al., 2015; Min et al., 2011). In the rapidly warming world of recent decades, changes in the climate at the global and regional level, and in temperature and precipitation extremes, have become increasingly detectable relative to background variability (e.g., Eyring et al., 2021; Seneviratne et al., 2021). However, local-scale changes have always been more challenging to robustly detect due to stronger variability on smaller spatial scales. As a result, attribution of climate changes has often been carried out at continental or large regional scales, particularly for studying causes of trends in extremes (e.g., Min et al., 2011, 2013; Paik et al., 2020; X. Zhang et al., 2013), so a signal may be extracted and confidently connected to anthropogenic influences. The detectability of regional and local climate changes under reduced greenhouse gas forcings or net zero emissions pathways remains an active area of research. Work to date has focused largely on the detection and de-emergence of rates of change (Borowiak et al., 2025), leaving the question of total change under net zero unexplored.

If greenhouse gas emissions are reduced, global warming will slow down, but the reduced rate of warming may be challenging to detect in the presence of background climate variability (MacDougall et al., 2024; Marotzke, 2019; McKenna et al., 2020). Projections from rapid decarbonization scenarios suggest a reduced cooling of the stratosphere may be one of the clearer signs of a response to reducing emissions in the near-term (Romanzini-Bezerra & Maycock, 2024). As climate changes slow under greatly reduced or net zero emissions, the expectation is that the land will generally cool while the ocean, particularly the Southern Ocean (Chamberlain et al., 2023), continues to warm (Armour et al., 2016; A. D. King et al., 2020; Long et al., 2020; Manabe et al., 1991). Other aspects of the climate system are expected to continue changing under net zero, with sea level rise (Mengel et al., 2018) and Antarctic sea ice extent decline (A. D. King et al., 2024) projected for centuries. Subtle changes in atmospheric circulation and precipitation patterns are also anticipated under low and net zero emissions pathways (Ceppi et al., 2018; Dittus et al., 2024; Grose & King, 2023; Sniderman et al., 2019). Under very strong decarbonization scenarios that are characterized by net negative emissions later this century, there is potential for some reduction in temperature and precipitation means, and extremes (Pfleiderer et al., 2024; Roldán-Gómez et al., 2025; Walton & Huntingford, 2024), but these changes may be masked by the inherent variability in extreme events and as a result be less apparent to people (Diffenbaugh et al., 2023).

Increasing greenhouse gas concentrations are currently causing major climate changes, however, in a post-net zero world these climate changes will likely be more subtle as they arise from the differing evolution and inertia of different parts of the Earth System. As humanity aims to reduce greenhouse gas emissions and reach net zero, it is worth considering whether these subtle changes will be easily identifiable and who may experience substantial regional and local changes. Furthermore, since current climate commitments are likely not sufficient to limit global warming to well below 2°C (United Nations Environment Programme, 2024), it is important to consider the effects of a delay in reaching net zero emissions on climate trends across spatial and temporal scales.

In this study, we use a bespoke set of seven millennial length net zero carbon dioxide emissions simulations run with an Earth System Model to examine the detectability of various changes in the climate system both in terms of time and delay in emissions cessation. While we discuss the detectability of the effects of delay in emissions cessation, these differences may also be framed in terms of additional cumulative carbon emissions. We provide the cumulative emissions associated with each simulation (Table 1) for ease of comparison and note additional cumulative emissions values when discussing effects of delay. This research increases understanding of changes in the climate system under net zero emissions and the effects of delay, as well as how apparent those changes may be.

Table 1
Cumulative Carbon Dioxide Emissions Associated With Each Net Zero Emissions Simulation Branching From SSP5-8.5

Year of emissions cessation	Cumulative carbon dioxide emissions (PgC)
2030	591
2035	666
2040	750
2045	845
2050	951
2055	1068
2060	1199

Note. Emissions are computed relative to 1750.

2. Data and Methods

There are a variety of experimental frameworks that have been developed in recent years which support analysis of slow-changing climate states under reduced carbon emissions (e.g., Jones et al., 2019). We analyzed the ACCESS-ESM-1.5 net zero carbon dioxide emissions simulations described by A. D. King et al. (2024) in this study. This is a set of seven 1000-year-long net zero emissions simulations that branch from an emissions-driven version of the shared socioeconomic pathway (SSP) 5–8.5 experiment (O'Neill et al., 2016) at 5-year intervals (2030, 2035, 2040, 2045, 2050, 2055, and 2060) with instantaneous carbon dioxide emissions cessation (see Table 1 for associated cumulative emissions). All other greenhouse gases and anthropogenic aerosol concentrations are returned to 1850 levels. Vegetation cover is held at the same level as the branching point with no further land use change throughout each net zero emissions simulation. The net zero simulations are hereafter referred to as "NZ" followed by the year of emissions cessation, for example "NZ2060" refers to the 1000-year net zero emissions simulation branching from SSP5-8.5 in 2060.

The purpose and framework for these simulations are described in detail in A. D. King et al. (2021) and A. D. King et al. (2024). We note these simulations are implausible in several ways, such as the instantaneous cessation of anthropogenic carbon dioxide emissions from a high level, and the return to 1850 levels for methane and nitrous oxide levels (Sowers et al., 2003; Z. Zhang et al., 2017, 2025). However, we believe this framework can be useful in understanding the general climate response to achieving net zero emissions.

As this framework is composed of a series of long net zero simulations each separated by 5 years of cumulative emissions (albeit, under a high emissions rate associated with SSP5-8.5), it enables a thorough analysis of the detectability of global, large-scale and local climate change indicators. The indices analyzed were:

- annual-average global mean surface temperature (GMST),
- annual-average regional and local surface temperatures,
- local annual maximum daily maximum temperatures (TXx),
- local annual minimum daily minimum temperatures (TNn),
- annual-average precipitation,
- local annual maximum daily total precipitation (Rx1day),
- the Atlantic Meridional Overturning Circulation (AMOC), calculated from the annual meridional stream-function at 26°N across the Atlantic basin,
- Arctic sea ice extent in September,
- and Antarctic sea ice extent in March.

The indices were calculated in the historical, SSP5-8.5, and seven 1000-year-long net zero emissions simulations. The 1850–1900 period in historical simulations was used as a proxy for a pre-industrial climate, and anomalies were computed from the average of this period.

To examine changes across scales, regional annual-average temperatures for the Intergovernmental Panel on Climate Change Sixth Assessment Report (IPCC AR6) regions were analyzed (Iturbide et al., 2020). We also investigated local changes using the grid-cells over the Melbourne region of Australia, Kinshasa in the Democratic Republic of Congo, and New York City in the United States as illustrative examples from different continents.

To test the detectability of changes both under a given net zero emissions pathway and as a function of delay in emissions cessation, the Kolmogorov-Smirnov test was used. The KS-test has been used commonly in climate change emergence analyses (A. D. King et al., 2015; Mahlstein et al., 2011, 2012) to estimate the probability of two samples being drawn from the same overall population. For this analysis, the detectability of changes under net zero emissions was examined by performing a KS-test comparing the first 30 years of each simulation with all subsequent 30-year periods. As these simulations involve a large, instantaneous change to net zero carbon dioxide emissions and 1850 levels of aerosols and other greenhouse gases, there is an initial shock associated with the abrupt reduction in radiative forcing (A. D. King et al., 2024). To account for this, an additional analysis where

years 101–130 (after the initial shock has passed) are compared with every subsequent 30-year period was also performed (Figures S2, S6–S10, and S12 in Supporting Information S1). For the examination of the effect of delay in emissions cessation on detectable climate changes, moving 30-year samples from the net zero simulation beginning in 2030 (NZ2030) were compared with equivalent 30-year samples from all other simulations also using a KS-test. For example, to understand the long-term effect of delay in emissions cessation, the period 971–1000 years into the NZ2030 simulation was compared with the period 971–1000 years into the net zero emissions simulation beginning in 2035, 2040, 2045, and so on. 30-year samples were used as this is a common definition of a climatology, with the use of different sample sizes affecting the detectability results but not the relative detectability of different climate change metrics. A detectable signal is defined as when the p-value of the KS-test statistic is less than 0.05. The KS-test is designed for use with independent samples, so the degrees of freedom were reduced where the lag-1 autocorrelation in a variable (based on the NZ2030 simulation after linear detrending) was positive using the equation:

$$n_{\text{eff}} \cong n \frac{1-\rho_1}{1+\rho_1}$$

following (Wilks, 2011), where n_{eff} is the effective sample size, n is the sample size, and ρ_1 is the lag-1 autocorrelation. This calculation was performed for global and regional-scale indices as well as at each location for the mean and extreme temperature and precipitation analysis.

Additionally, area and population exposure to detectable local climate changes were estimated. For this part of the analysis, the temperature and precipitation indices were regridded to a regular 2° grid using a bilinear interpolation for temperature indices and a conservative remapping for precipitation indices. The area with detectable changes, as a function of time or delay in emissions cessation, was computed as the percentage of the surface where the p-value from the KS-test was less than 0.05. Gridded population data on a 0.5° grid based on 2020 estimates were obtained from the NASA Socioeconomic Data and Applications Centre ("Basic Demographic Characteristics, v4.11: Gridded Population of the World (GPW), v4," 2018). The population data was summed onto the same regular 2° grid, and the population in locations of detectable changes was aggregated. While population changes will occur and differ in future along with scenarios for climate change, using 2020 estimates gives an indication of where detectable changes are projected to occur relevant to the current population distribution.

3. Results

The net zero carbon dioxide emissions simulations are characterized by slow global warming over the course of the 1000-year runs with a marked distinction in GMST between the simulations, demonstrating a strong effect of delayed emissions cessation (or additional cumulative emissions) both initially and in the longer term (Figures 1a and 1b). There is a complete separation of the histograms of annual-average GMST when emission cessation is delayed by 30 years (noting that because these simulations branch from SSP5-8.5 this corresponds to a difference of 608 PgC cumulative emissions). This complete separation persists such that more than 900 years after cessation, the effect of delay in emissions cessation on GMST is as apparent as at the beginning of the simulation (Figure 1b). However, greater variability at regional and local scales (Hawkins & Sutton, 2009; Lehner & Deser, 2023), as seen for the examples of Southern Australia (SAU) (Figures 1c and 1d), the grid-cell over the Melbourne region (Figures 1e and 1f), and for extreme indices such as TXx (Figures 1g and 1h) makes the effect of delayed emissions cessation less clear. The rate of warming in the SAU region is marked and slightly stronger in the NZ2060 simulation than the NZ2030 simulation with complete separation between histograms from these simulations near the end of the 1000-year period but not at the beginning (Figure 1d). There remains a marked effect of delayed emissions cessation and slow warming at the Melbourne grid-cell, but high values of TXx at the beginning of the NZ2030 simulation remain inside, albeit at the cooler end, of the distribution at the end of the NZ2060 simulation. The distributions of TXx (Figure 1h) are also significantly different based on a KS-test (p-value < 0.05) but are illustrative of the increased challenge in detection of trends or delayed emissions cessation in local extreme indices relative to local mean (Figure 1f), regional mean (Figure 1d), or global mean (Figure 1b).

10.1029/2025EF006918

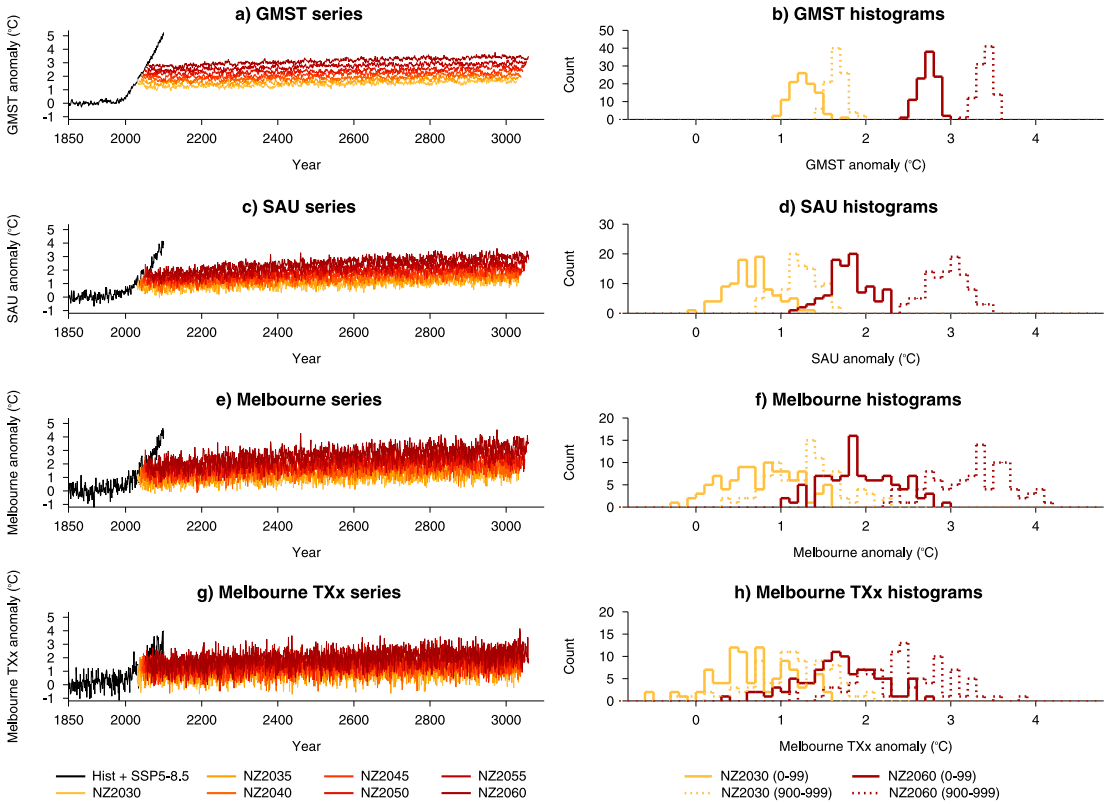

Figure 1. Timeseries of (a) global annual average temperature anomalies, (c) Southern Australia (SAU) annual average temperature anomalies, (e) Melbourne annual average temperature anomalies and (g) Melbourne annual maximum daily maximum temperature anomalies in ACCESS-ESM-1.5 historical and SSP5-8.5 r10i1p1f1 simulations (black) and 1000-year-long net zero emissions simulations starting at 5-year intervals from 2030 to 2060 (grading from yellow to red). Histograms of (b) global annual average temperature anomalies, (d) SAU annual average temperature anomalies, (f) Melbourne annual average temperature anomalies and (h) Melbourne annual maximum daily maximum temperature anomalies in the first 100 years of the net zero simulation starting in 2030 (yellow), the last 100 years of the net zero simulation starting in 2030 (yellow dotted), the first 100 years of the 2060 net zero simulation (red) and the last 100 years of the 2060 net zero simulation (red dotted). All anomalies are from an 1850–1900 baseline.

3.1. Detectability of Changes Under Net Zero Emissions

Throughout each net zero emissions simulation, detectable changes in climate variables relative to the climate immediately following emissions cessation gradually become apparent across scales. The warming in global mean annual-average temperatures becomes detectable over the course of the simulations, particularly in the simulations where emission cessation is delayed (Figures 2a and 2b). There is an initial cooling in these simulations due to non-CO_2 greenhouse gas concentrations returning to 1850 levels (A. D. King et al., 2024) and the effect of this is more pronounced in the earlier net zero runs. Figure S2 in Supporting Information S1 shows equivalent results using only the period 100 years post emissions cessation onwards. In that case the short-term cooling is removed but the long-term warming effect remains evident.

Other large-scale climate indices are also characterized by detectable changes over the course of the simulations. Atlantic Meridional Overturning Circulation (AMOC) changes are known to be highly variable between models under net zero emissions (Jackson et al., 2014; MacDougall et al., 2022). In the ACCESS-ESM-1.5 model, there is a slight recovery in AMOC that becomes detectable within two to three centuries in most net zero emissions simulations (Figures 2c and 2d) similar to previous findings in several single model studies (Lacroix et al., 2024; Schwinger, Asaadi, Goris, et al., 2022; Schwinger, Asaadi, Steinert, et al., 2022). For context, the AMOC decline in SSP5-8.5 up to 2100 in ACCESS-ESM-1.5 is weaker than in most other models (Weijer et al., 2020) in the sixth phase of the Coupled Model Intercomparison Project (Eyring et al., 2016).

Arctic seasonal minimum sea ice extent generally shows some recovery from the initial post-emissions cessation period, although this is subtle and variable between simulations (Figures 2e and 2f). For the simulations where emissions cessation is later (NZ2050, NZ2055 and NZ2060), Arctic sea ice extent starts at very low levels and

10.1029/2025EF006918

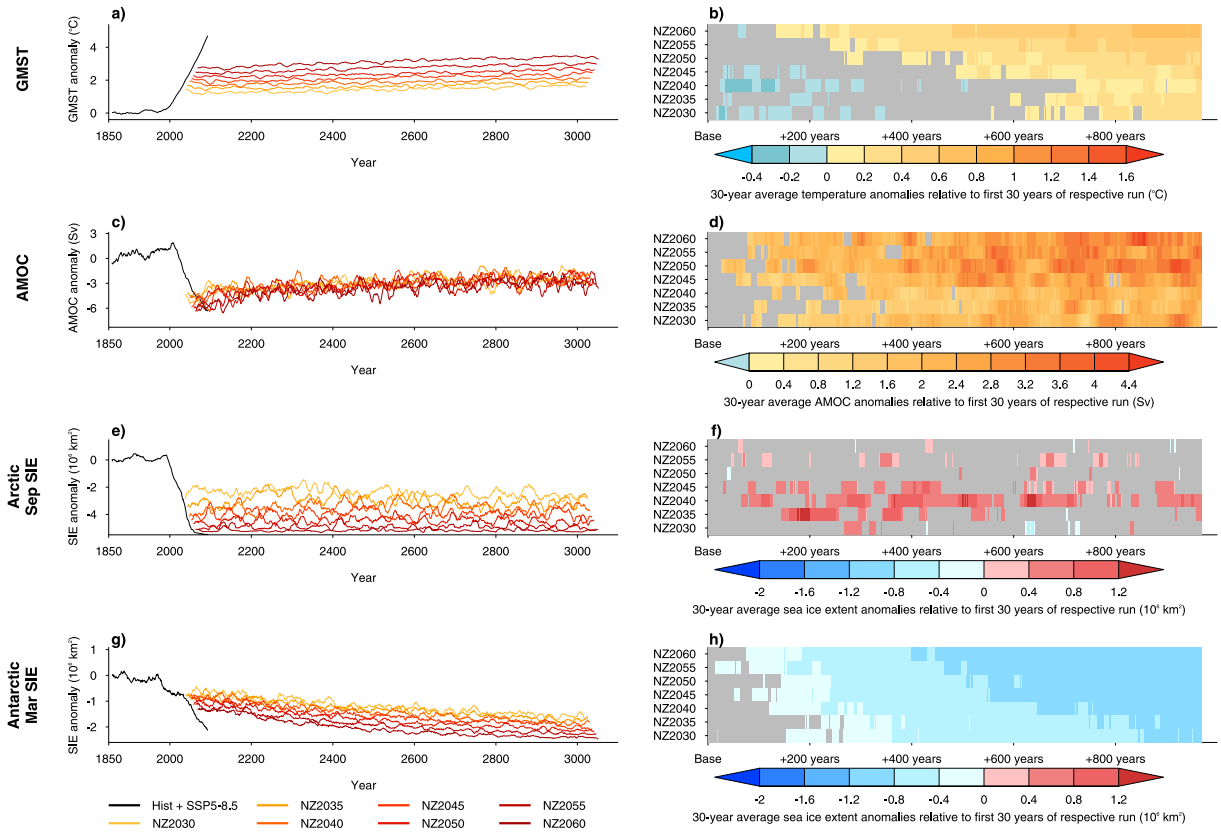

Figure 2. Timeseries of 11-year smoothed (a) global annual average temperature anomalies, (c) Atlantic Meridional Overturning Circulation (AMOC) index, (e) Arctic sea ice extent in September and (g) Antarctic sea ice extent in March in ACCESS-ESM-1.5 historical and SSP5-8.5 r10i1p1f1 simulations (black) and 1000-year-long net zero emissions simulations starting at 5-year intervals from 2030 to 2060 (grading from yellow to red). Difference between the average of the first 30 years of each net zero simulation and all subsequent 30-year averages in each net zero emissions simulation for (b) global-mean surface temperature (GMST), (d) AMOC index, (f) Arctic sea ice extent in September, and (h) Antarctic sea ice extent in March. Gray rectangles indicate the difference between the 30-year period and the first 30 years of that simulation is non-significant ($p < 0.05$) using a Kolmogorov-Smirnov test.

appears to remain in a regime of being virtually sea ice free in September (A. D. King et al., 2024). In contrast, Antarctic sea ice extent decline continues under net zero emissions and is stronger and more detectable when emissions cessation occurs later (Figures 2g and 2h).

Regional temperature changes are diverse with many Northern Hemisphere areas cooling significantly under net zero emissions, while Southern Hemisphere regions continue to warm and tropical regions experience little change (Figure 3, Figures S3–S5 in Supporting Information S1). Continued Southern Ocean warming (and associated warming of Southern Hemisphere land areas) post-net zero has been identified previously (Chamberlain et al., 2023). As for GMST, SAU warms substantially and more so in the delayed emissions cessation simulation (NZ2060) (Figures 3a and 3b). There is an initial cooling evident in most regions due to non-CO_2 greenhouse gas concentrations returning to 1850 levels. Figures S6–S9 in Supporting Information S1 show equivalent results using only the period 100 years post emissions cessation onwards.

Changes in mean and extreme indices at the grid-cell scale are noisier and the detectability of changes is reduced (Figure 4), however the overall pattern of warming in Melbourne and cooling in New York is still evident in some simulations. Changes in Rx1day at the gridcell scale under net zero emissions are also highly variable between simulations (Figures 4m–4o). The noisiness, and by construction, rarity, of extreme events can mean that changes do not become readily apparent even in the presence of an underlying trend (Diffenbaugh et al., 2023; Zeder et al., 2023). The use of a baseline period a century later (Figure S10 in Supporting Information S1) also highlights this noisiness with results differing for a given simulation, especially for TNn and Rx1day, with a shift in baseline.

Figure 5 shows the pattern of mean temperature and precipitation changes during the NZ2030, NZ2040, NZ2050 and NZ2060 simulations, with Figure S11 in Supporting Information S1 showing equivalent changes in TXx and

10.1029/2025EF006918

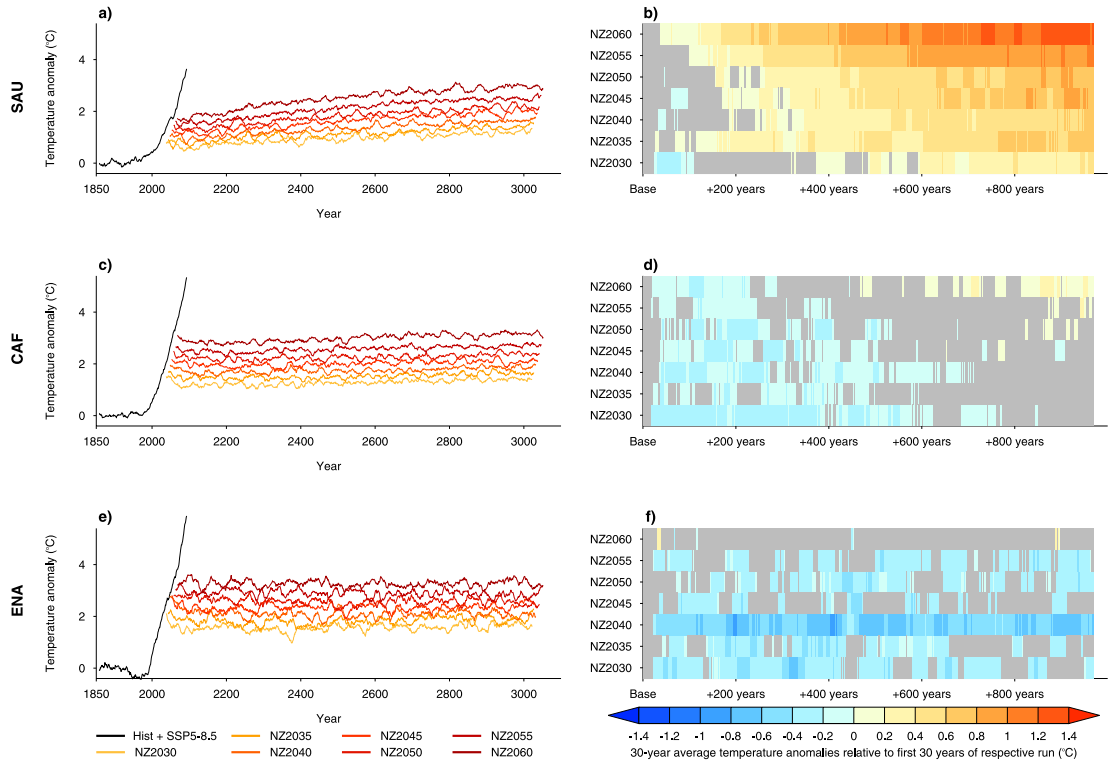

Figure 3. As Figure 2 but for surface temperature anomalies averaged across select IPCC reference regions; (a), (b) Southern Australia, (c), (d) Central Africa, and (e), (f) Eastern North America.

Rx1day. There are consistent signals across the simulations of strong warming over the Southern Ocean. This warming is detectable relative to background variability and strengthens even between the middle and end of the 1000-year simulations (Figures 5a, 5b, 5e, 5f, 5i, 5j, 5m, and 5n). This strong Southern Ocean warming under low or net zero emissions has been noted previously (e.g., Armour et al., 2016; Chamberlain et al., 2023; A. D. King et al., 2024). In contrast, many Northern Hemisphere land regions, particularly inland areas, show significant cooling under net zero emissions. Generally, these patterns of change are more marked in the delayed emissions cessation cases, although it should be noted that they start from a point of higher temperatures than the earlier cessation simulations.

Precipitation changes under net zero emissions are generally less spatially coherent but are detectable in some regions. Significant increases are identified over the Southern Ocean and Antarctica in particular (Figures 5c, 5d, 5g, 5h, 5k, 5l, 5o, and 5p). These changes are also clearer at the end than in the middle of the simulations, indicative of changes occurring long after emissions cessation. The detectability of precipitation changes is also clearer in the NZ2050 and NZ2060 simulations relative to NZ2030 and NZ2040. Under delayed emissions cessation there is a larger increase in global-average precipitation (A. D. King et al., 2024) which helps to explain the larger areas of detectable increase in NZ2060 relative to the other simulations (Figures 5c and 5d).

Changes in extreme indices under net zero emissions are largely similar to changes in the means (Figure S11 in Supporting Information S1). There are widespread detectable changes in TXx at the grid-cell level, particularly with respect to the warming over the Southern Ocean and cooling over some mid-latitude land areas in the Northern Hemisphere. Rx1day changes are less spatially coherent and detectable than mean precipitation changes during the net zero emissions simulations.

Figure 6 shows aggregates of area and population in locations of detectable changes in mean and extreme climate indices. The slow continued global warming under net zero emissions is accompanied by an increasing area of detectable local warming and a decreasing area of detectable cooling (Figure 6a). As most of the warming signal is over the ocean, this does not translate into a large proportion of the population residing in locations of detectable warming, with more people living in locations of significant cooling than warming (Figure 6e). There is some

10.1029/2025EF006918

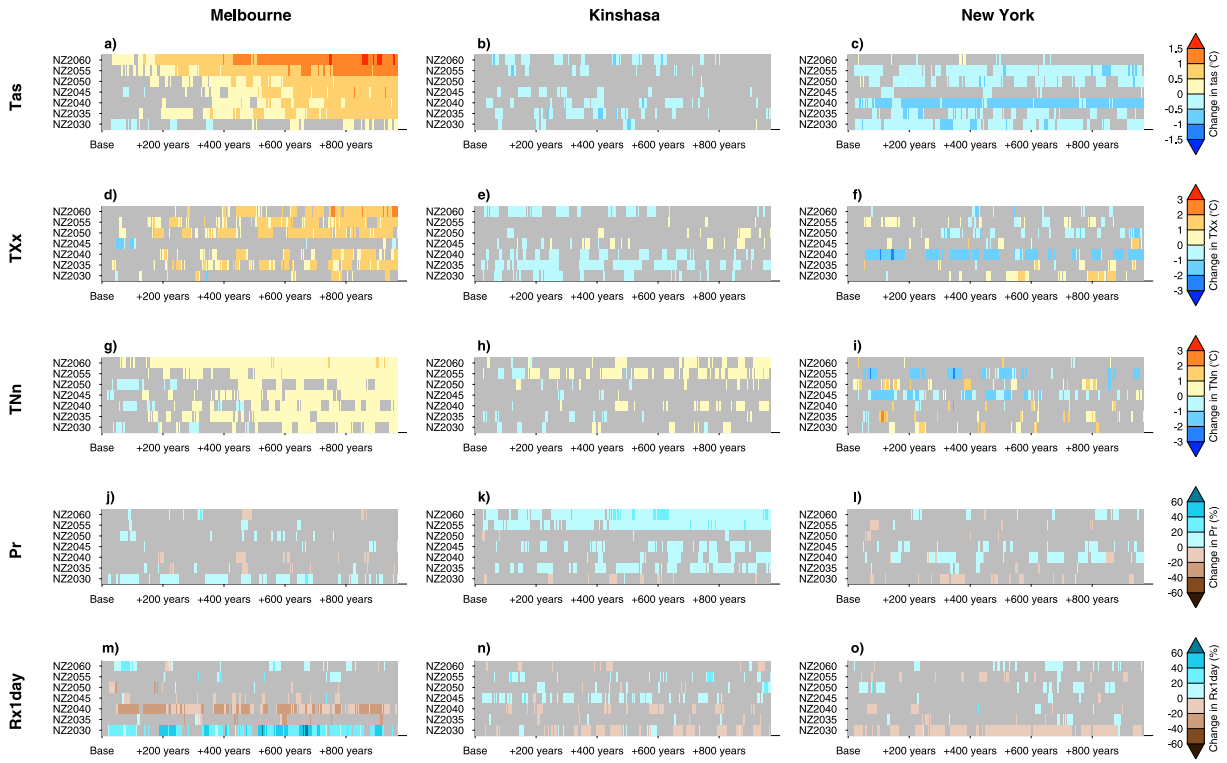

Figure 4. Difference between the average of the first 30 years of each net zero simulation and all subsequent 30-year averages in each net zero emissions simulation for (a–c) mean annual temperature, (d–f) annual maximum daily maximum temperature (TXx), (g–i) annual minimum daily minimum temperature (TNn), (j–l) annual total precipitation, and (m–o) annual maximum daily precipitation (Rx1day) in Melbourne, Kinshasa and New York City gridcells, respectively. Gray rectangles indicate the difference between the 30-year period and the first 30 years of that simulation is non-significant ($p < 0.05$) using a Kolmogorov-Smirnov test.

difference in population exposure to detectable changes between simulations. When emissions cessation is delayed we find more people live in places of detectable local warming and fewer people live in places of detectable local cooling. This is associated with a slightly higher rate of global warming in the simulations where emissions cessation is later. Delaying the baseline from which detectability is examined by a century (Figure S12 in Supporting Information S1) decreases the area and population exposure to significant cooling. It is again worth noting that these simulations are idealized in the way emissions cessation is imposed, but the results are indicative of expected changes and the places and people that would experience such changes post-net zero.

For precipitation, a larger area of the world undergoes significant local increases than decreases under net zero emissions (Figure 6b), but more people reside in locations of significant precipitation decrease than increase (Figure 6f). This is due to the precipitation increases occurring more over ocean than land (Figure 5). Area and population exposure to changes in temperature and precipitation extremes largely follow those of temperature and precipitation means, respectively (Figures 6c, 6d, 6g, and 6h).

3.2. Detectability of Differences Due To Delayed Emissions Cessation

A delay in ceasing emissions, relative to cessation in 2030, has detectable consequences on global and local climate indices (Figure 7). Even short delays in emissions cessation have a significant warming effect on global-average temperatures (Figure 7a), noting that a 5-year delay equates to an additional 74 PgC emissions due to the branching from the high emissions SSP5-8.5 simulation (A. D. King et al., 2024). For AMOC, there is a similar recovery in all simulations with few detectable and significant differences identified (Figure 7b). Arctic and Antarctic sea ice both have detectable, significant decreases in extent with only 10–15 years delay (at SSP5-8.5 emissions levels) in emissions cessation (Figures 7c and 7d).

At the regional level the effects of delay in emissions cessation are detectable and substantial across all the IPCC reference regions (Figure 8; others not shown). Even at the local level, differences in average temperatures are

10.1029/2025EF006918

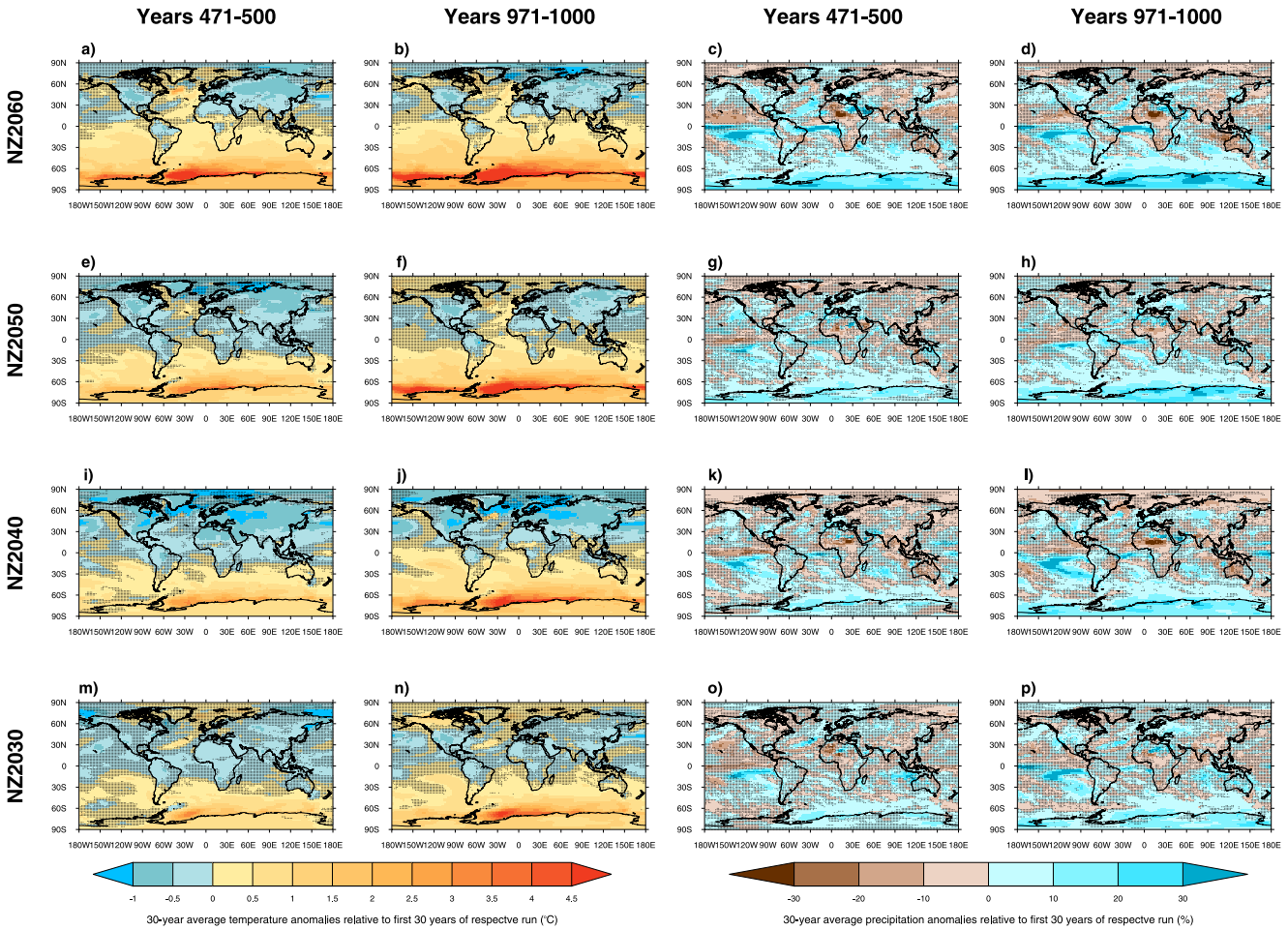

Figure 5. Maps of change in (a, b, e, f, i, j, m, and n) annual-average temperature and (c, d, g, h, k, l, o, and p) annual total precipitation between the first 30 years of the (a–d) NZ2060, (e–h) NZ2050, (i–l) NZ2040, and (m–p) NZ2030 simulation and years 471–500 and 971–1000 years after emissions cessation in those simulations, respectively. Stippling indicates locations where the difference between that 30-year period and the first 30 years of that simulation is non-significant ($p < 0.05$) using a Kolmogorov-Smirnov test.

detectable with short delays in emissions cessation (Figures 9a–9c). For extreme temperature indices, the increased variability masks some of the effects of delayed emissions cessation (Figures 9d–9i), but generally we see that a 10-15-year delay (SSP5-8.5 emissions levels) has significant and detectable effects on TXx and TNn. Changes in Rx1day are so small relative to internal variability that there is little detectable effect of delayed emissions cessation on this index (Figures 9m–9o).

Relative to net zero emissions from 2030 onwards, there is widely detectable warming across most of the planet when emissions cessation occurs later (Figure 10). Delaying emissions cessation by just 10–20 years (equivalent to an additional 159–359 PgC cumulative emissions), assuming an underlying SSP5-8.5 emissions scenario, has a significant effect on temperatures across almost all regions for many centuries and in some areas, such as the Southern Ocean, the difference even grows over time. Similarly, persistent effects of delay in emissions cessation are detectable for precipitation over many areas, especially Antarctica and the Southern Ocean, but not for most inhabited areas. The effects of delay in emissions cessation on extremes follow a similar pattern to that seen in the means (Figure S13 in Supporting Information S1). However, for both TXx and Rx1day, the detectability of these differences is reduced in many places compared to mean temperature and precipitation.

Relative to the NZ2030 simulation, delayed emissions cessation results in large areas of detectable warming and this signal lasts throughout the 1000-year-long simulations (Figure 11a). Even with only a 5-year delay (additional 74 PgC cumulative emissions), 51% of the world is significantly warmer on average and this increases to 84% for a 10-year delay (additional 159 PgC cumulative emissions) and almost 100% for a 30-year delay

10.1029/2025EF006918

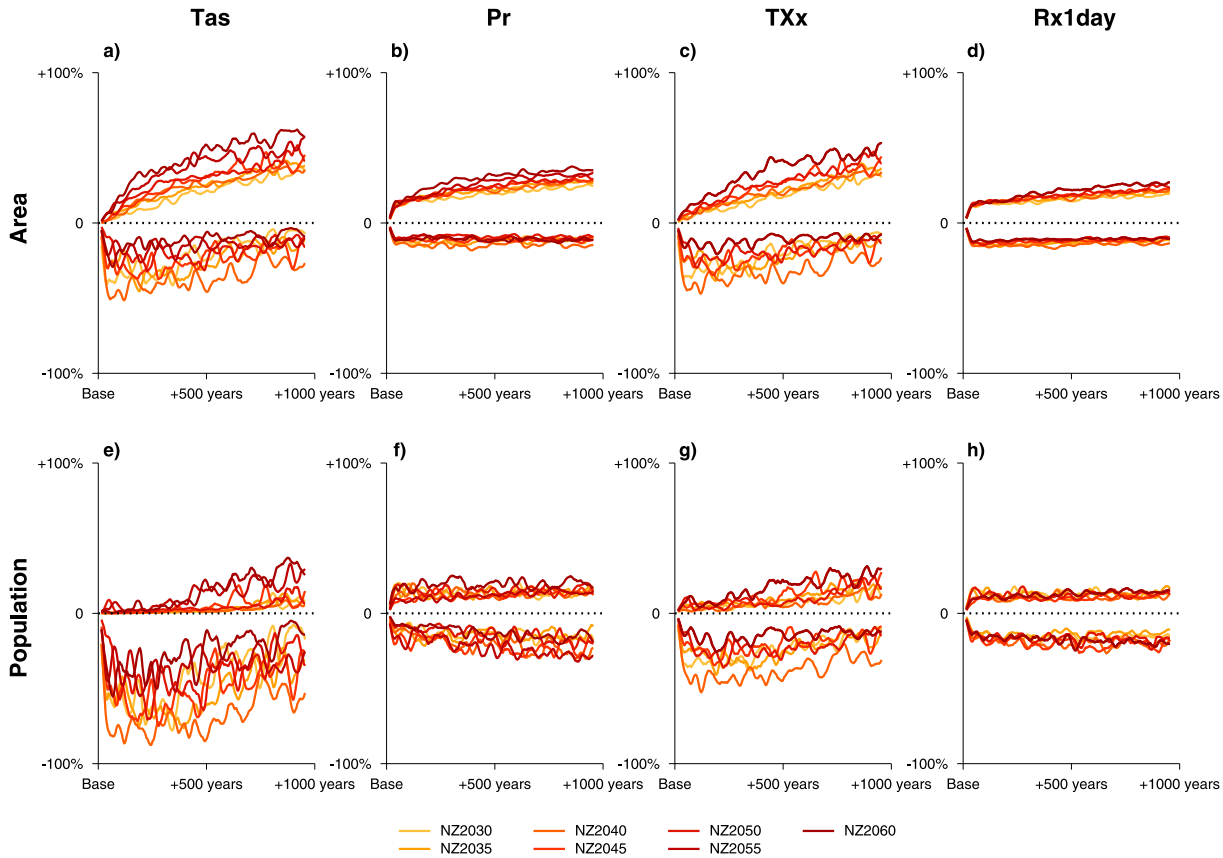

Figure 6. Timeseries of area and population exposure to detectable changes over time under net zero emissions. (a–d) Timeseries of percentage of global surface where (a) annual-average temperature, (b) annual total precipitation, (c) annual maximum daily maximum temperature, and (d) annual maximum daily precipitation totals are significantly different from the first 30 years after emissions cessation in each simulation. Values above the dashed lines indicate areas of significant change with an increase (i.e., warming or increasing precipitation) and below the dashed line represent significant change with a decrease (i.e., cooling or decreasing precipitation). (e–h) Timeseries of global population exposure (as a percentage) to significant changes in (e) annual-average temperature, (f) annual total precipitation, (g) annual maximum daily maximum temperature, and (h) annual maximum daily precipitation totals. A 30-year moving average has been applied to all timeseries.

(additional 608 PgC cumulative emissions). For TXx, the equivalent numbers are only slightly lower (41% for 5-year delay/74 PgC additional emissions, 69% for 10-year delay/159 PgC additional emissions, and 96% for 30-year delay/608 PgC additional emissions). The population exposure to detectable increases in local temperature with a delay in emissions cessation is generally similar for both temperature and TXx (Figures 7e and 7g).

Precipitation and Rx1day follow a more complex pattern of detectable increases in some areas and decreases in others when emissions cessation is delayed (Figures 11b and 11d). Overall though, there are more locations of significant increase than decrease in mean precipitation and Rx1day. This translates to more people in locations of detectable increased mean and extreme precipitation than decreases in these idealized simulations. Population exposure to increased Rx1day when net zero emissions is delayed is greater than for mean precipitation (33% and 22% respectively for the NZ2060 simulation on average).

4. Discussion and Conclusions

There is a growing need to understand the consequences for the climate of achieving net zero emissions and the long-term implications of any delay in reaching net zero (otherwise framed as additional cumulative carbon emissions prior to emissions cessation). In this study, we examine the detectability of such changes using a selection of global, regional and local climate change indicators. This is not an exhaustive set of climate indices, and there are other modeling frameworks and methods that could be used, but we believe this is a useful step in understanding climate evolution under net zero emissions and the effects of delayed cessation, across temporal and spatial scales.

10.1029/2025EF006918

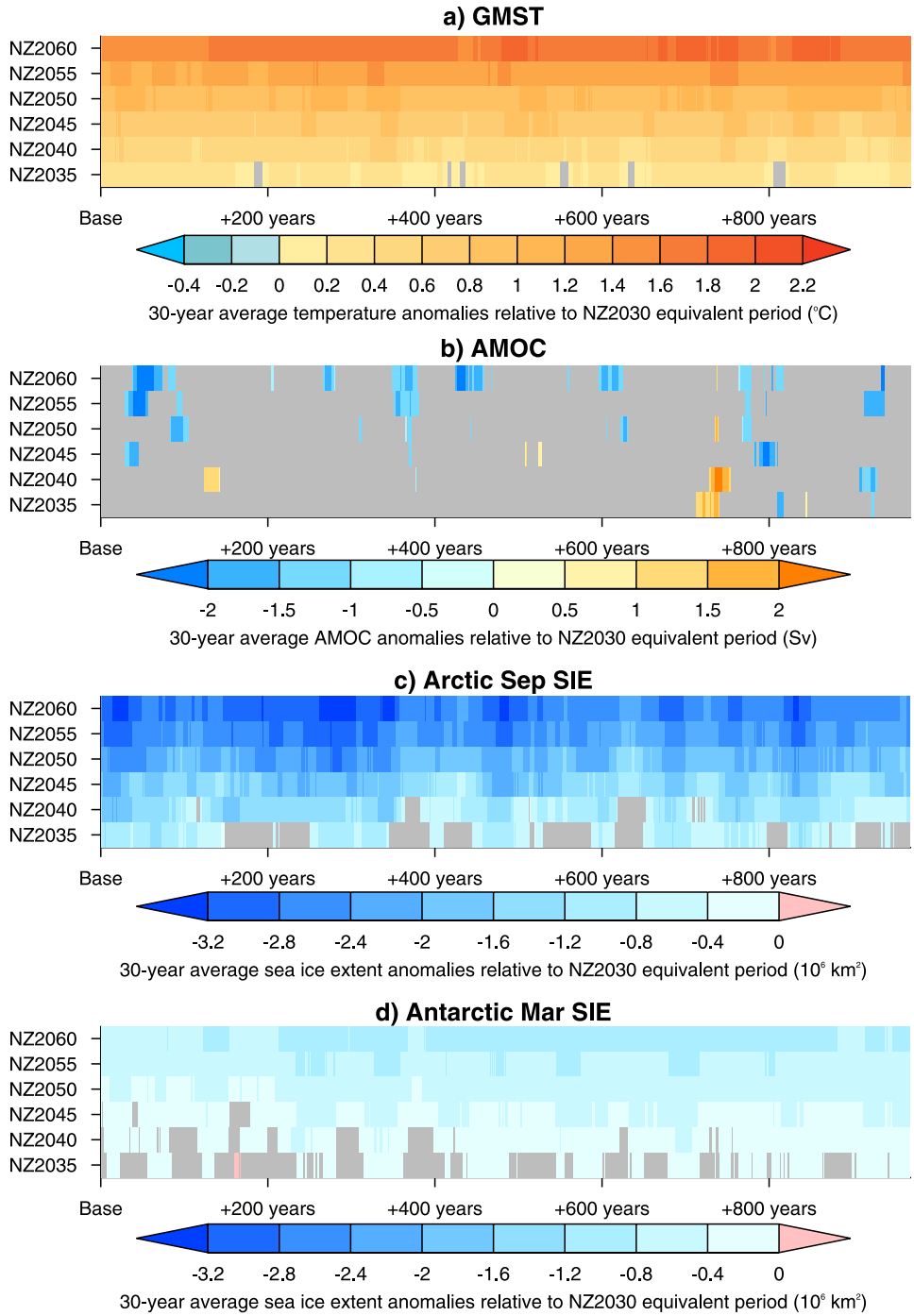

Figure 7. As Figures 2b, 2d, 2f, and 2h but differences are shown relative to the equivalent 30-year period in the simulation where emissions cease in 2030 (NZ2030).

This study makes use of a highly idealized experimental setup with instantaneous net zero carbon dioxide emissions achieved at different points in the 21st century branching from a very high emissions scenario (SSP5-8.5). There is a growing body of evidence that suggests SSP5-8.5 is implausible given the current global greenhouse gas emissions trajectory (Hausfather, 2025; Huard et al., 2022; Sarofim et al., 2024). While this scenario was useful to run distinct net zero scenarios branching from different years, it should be noted that a 5-year delay in emissions cessation in this framework is not reflective of a 5-year delay between plausible net zero emissions scenarios. We also note the implausibility of other aspects of our net zero model experiments, including

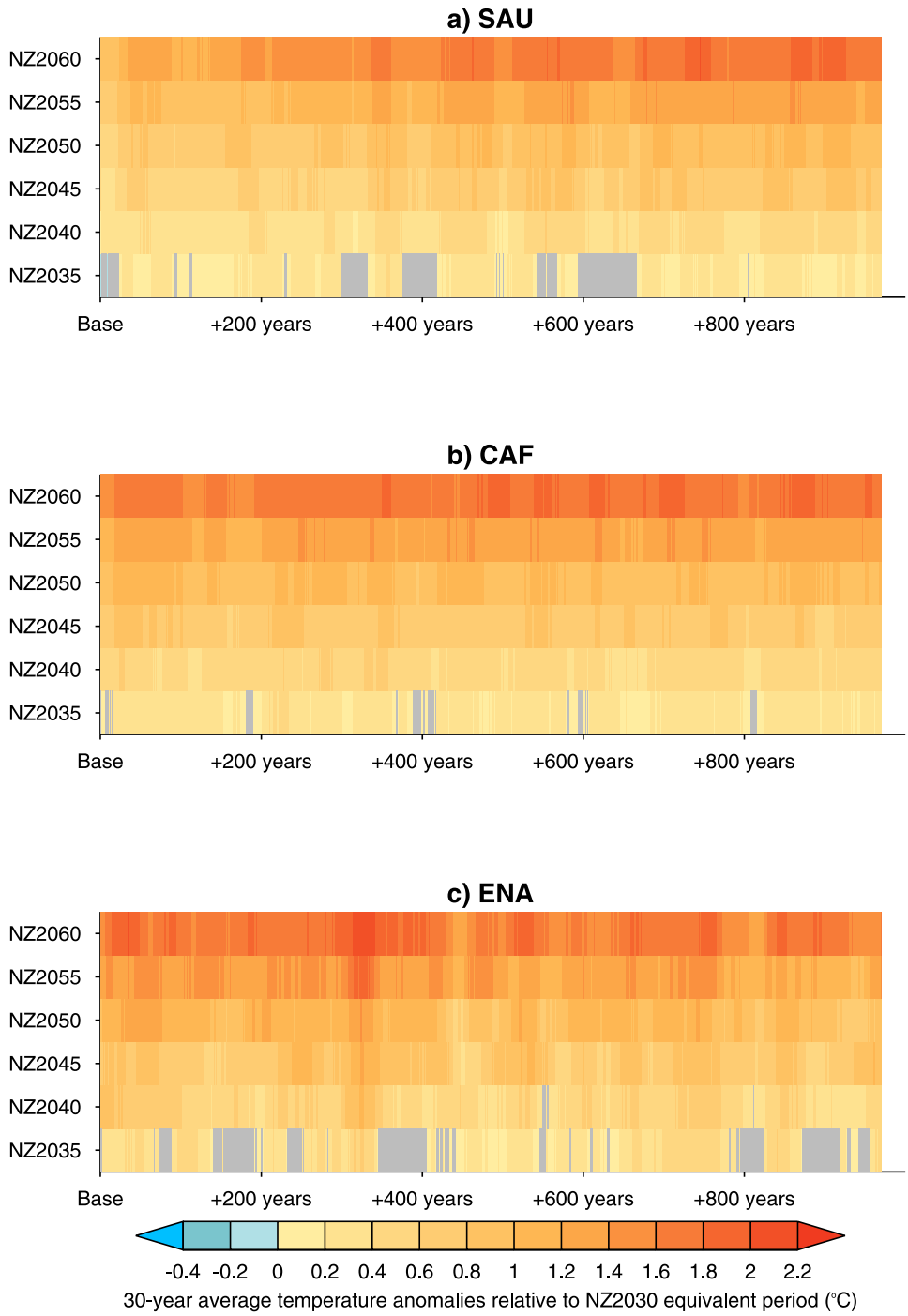

Figure 8. As Figures 3b, 3d, and 3f but differences are shown relative to the equivalent 30-year period in the simulation where emissions cease in 2030 (NZ2030).

the return to 1850 levels of non-carbon dioxide greenhouse gas concentrations where there is evidence that this is unlikely (Sowers et al., 2003; Z. Zhang et al., 2017, 2025). Analysis of plausible scenarios would be beneficial but is limited at the present by a lack of diversity and the short length of the current generation of scenario-based climate projections (O'Neill et al., 2016).

Under net zero carbon dioxide emissions, we found detectable changes not only in GMST, but also in local temperature means and extremes, especially over the Southern Ocean (with continued warming) and mid-latitude

10.1029/2025EF006918

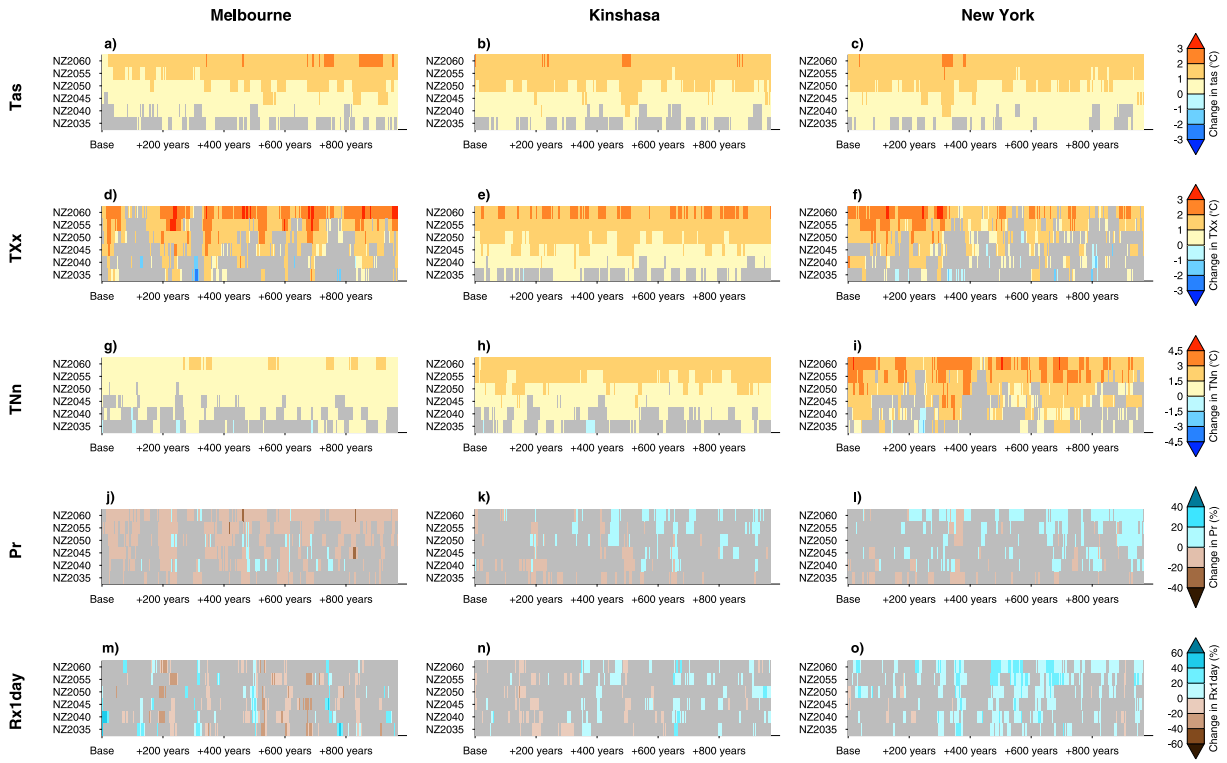

Figure 9. As Figure 4 but differences are shown relative to the equivalent 30-year period in the simulation where emissions cease in 2030 (NZ2030).

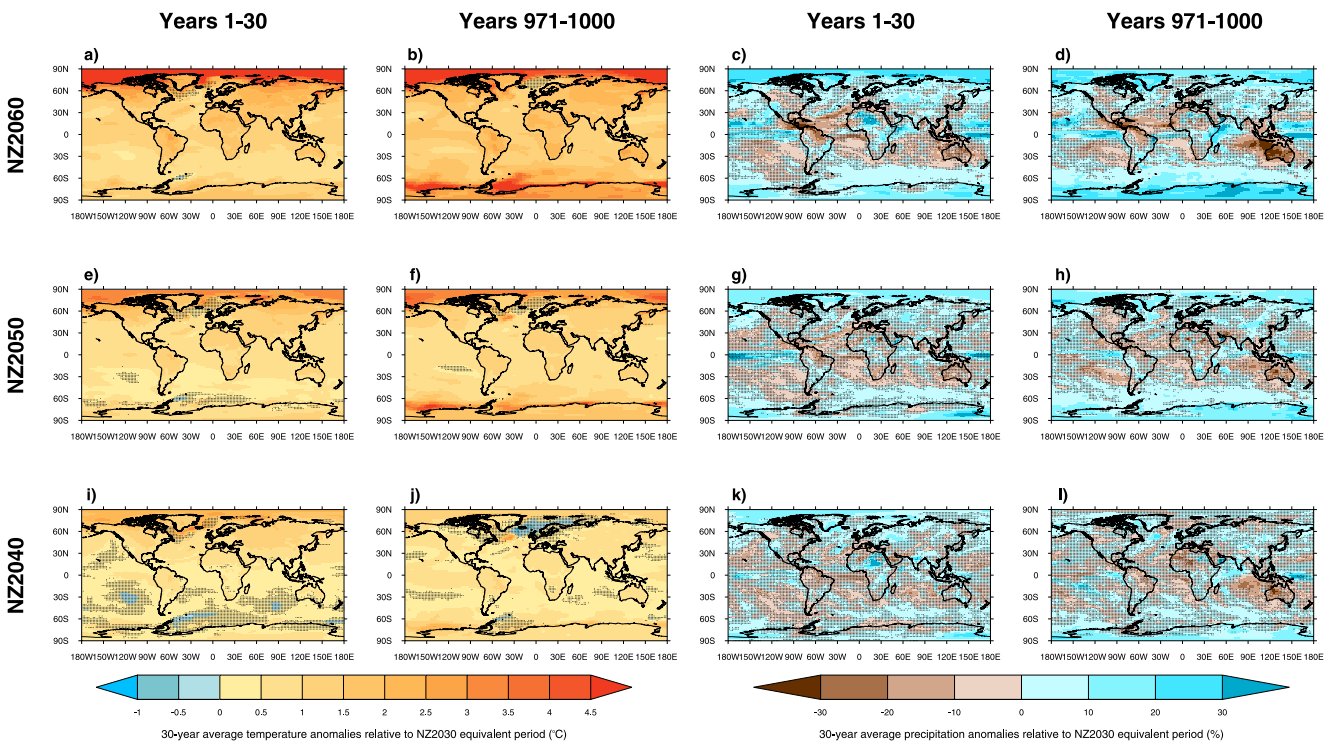

Figure 10. Maps of change in (a, b, e, f, i, and j) annual-average temperature and (c, d, g, h, k, and l) annual total precipitation between 30-year averages in the (a–d) NZ2060, (e–h) NZ2050, and (i–l) NZ2040 simulation and the equivalent 30-year average for the NZ2030 simulation. Stippling indicates locations where the difference between that 30-year period and the equivalent 30 years of the NZ2030 simulation is non-significant ($p < 0.05$) using a Kolmogorov-Smirnov test.

10.1029/2025EF006918

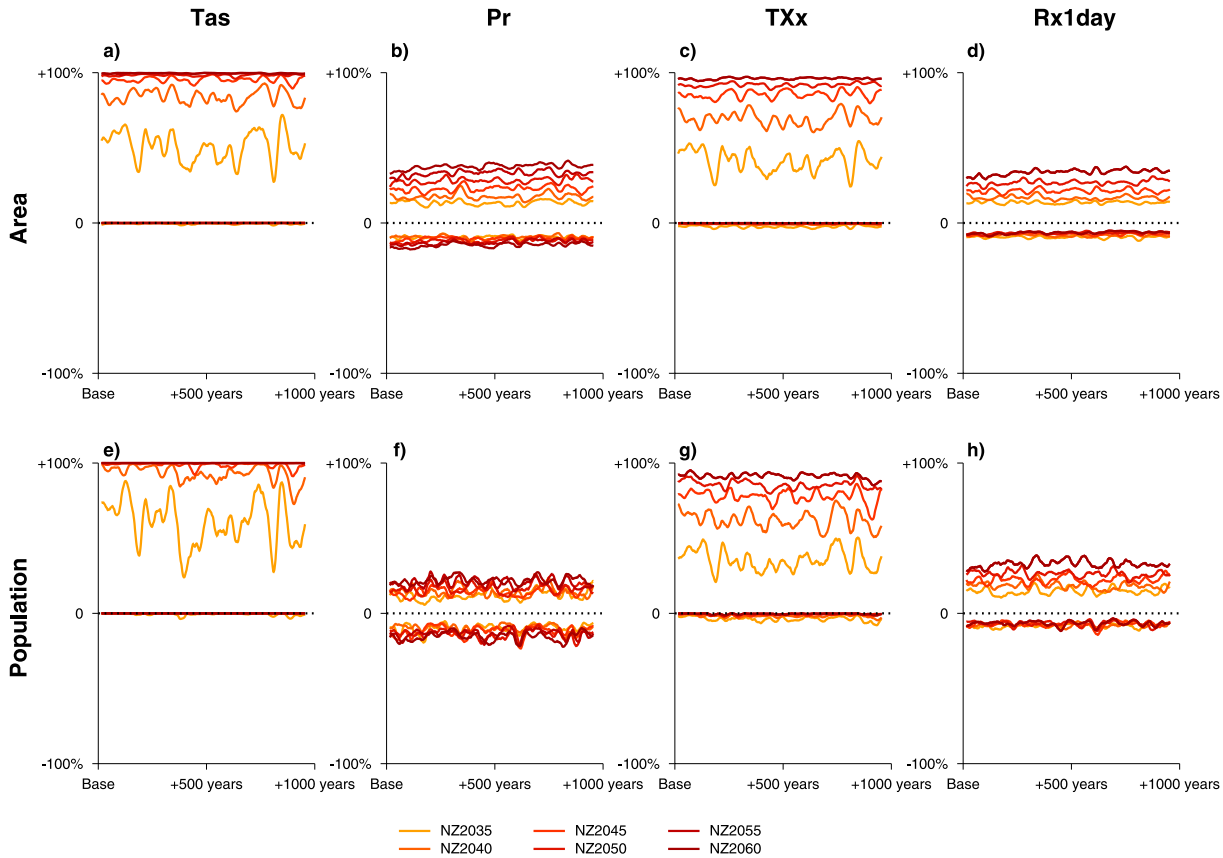

Figure 11. As Figure 6 except changes are relative to a moving NZ2030 baseline rather than the start of each simulation.

land regions (cooling). To a lesser extent, detectable changes in precipitation means and extremes were identified (e.g., increases over Antarctica). Over centuries, recovery in AMOC and decline in Antarctic sea ice extent are also detectable. In some of these cases, the changes represent the continuation of current trends with negative consequences (e.g., ocean warming and Antarctic sea ice decline) highlighting how even with aggressive emissions reduction some major changes in the climate system should be expected to continue (A. D. King et al., 2025).

We found that delaying carbon dioxide emissions cessation, equivalent to increasing cumulative emissions prior to cessation, has a detectable effect on global and local temperatures and sea ice extent in both the Arctic and Antarctic. Mean and extreme precipitation changes in some locations, particularly high-latitude regions, are also detectable if emissions cessation is delayed by 10–20 years (in an underlying scenario following SSP5-8.5 emissions levels).

This study highlights that reaching net zero emissions sooner is highly beneficial and that delays will have large long-term effects both globally and locally. However, remaining at net zero emissions over long periods, rather than achieving substantial net negative emissions (A. D. King et al., 2022; Schleussner et al., 2024), also poses long-term climate risks as some aspects of the Earth system, such as Antarctic sea ice extent, continue to drift further away from their pre-industrial state. The changes in temperature under net zero emissions are significant in many areas and more so in the mid-to-high latitudes than near the equator. This contrasts with the spatial pattern of warming in the current climate which is strongest in low-latitude areas (e.g., Mahlstein et al., 2011).

Further work to understand the implications of net zero emissions across timescales (decades through to millennia) is needed. This study suggests even scenarios with subtle differences in forcings may lead to detectable global and local differences in climate states, but further exploration of this issue in the next set of global climate model projections (van Vuuren et al., 2025), including in net zero scenarios, is needed. Comprehensive analyses of climate changes under net zero emissions and the consequences of delay will be needed to support robust policymaking.

Conflict of Interest

The authors declare no conflicts of interest relevant to this study.

Data Availability Statement

All model simulations are available on the Australian node of the Earth System Grid Federation. The historical simulations are available at Ziehn et al. (2019a). The SSP5-8.5 simulations are available at Ziehn et al. (2019b). The net zero emissions simulations used in this analysis are available at A. King (2024). The code used to perform this analysis is available at A. King (2025).

Acknowledgments
ADK, SC, and NM received funding from the Australian Research Council (CE230100012). ADK also received funding from the Australian Research Council Future Fellowship program (FT240100306). NM also received funding the Australian Research Council DECRA program (DE230100315). ADK and TZ acknowledge the Australian Government National Environmental Science Program. EAdA acknowledges funding by the Deutsche Forschungsgemeinschaft (DFG, German Research Foundation) under Germany's Excellence Strategy—EXC 2037 "CLICCS- Climate, Climatic Change, and Society"—Project Number: 390683824. The authors also acknowledge the Australian National Computing Infrastructure (NCI) for providing data access and computational resources used in this study.

References

Armour, K. C., Marshall, J., Scott, J. R., Donohoe, A., & Newsom, E. R. (2016). Southern Ocean warming delayed by circumpolar upwelling and equatorward transport. *Nature Geoscience*, *9*(7), 549–554. https://doi.org/10.1038/ngeo2731

Basic Demographic Characteristics, v4.11: Gridded Population of the World (GPW), v4. (2018). *Basic demographic characteristics, v4.11: Gridded population of the world (GPW), v4*. NASA Socioeconomic Data and Applications Center (SEDAC). Retrieved from https://sedac.ciesin.columbia.edu/data/set/gpw-v4-basic-demographic-characteristics-rev11

Borowiak, A., King, A. D., Brown, J. R., Jones, C. D., & Grose, M. (2025). Climate stabilisation under net zero CO2 emissions. *Earth's Future*, *13*(3), e2024EF005678. https://doi.org/10.1029/2024EF005678

Borowiak, A., King, A. D., Brown, J. R., Jones, C. D., Ziehn, T., Meinshausen, M., & Cassidy, L. (2024). Projected global temperature changes after net zero are small but significant. *Geophysical Research Letters*, *51*(8), e2024GL108654. https://doi.org/10.1029/2024GL108654

Cassidy, L. J., King, A. D., Brown, J., MacDougall, A. H., Ziehn, T., Min, S.-K., & Jones, C. D. (2023). Regional temperature extremes and vulnerability under net zero CO2 emissions. *Environmental Research Letters*, *19*(1), 014051. https://doi.org/10.1088/1748-9326/AD114A

Ceppi, P., Zappa, G., Shepherd, T. G., & Gregory, J. M. (2018). Fast and slow components of the extratropical atmospheric circulation response to CO2 forcing. *Journal of Climate*, *31*(3), 1091–1105. https://doi.org/10.1175/JCLI-D-17-0323.1

Chamberlain, M. A., Ziehn, T., & Law, R. M. (2023). The Southern Ocean as the freight train of the global climate under zero-emission scenarios with ACCESS-ESM1.5. *Biogeosciences Discussions*, 1–29. https://doi.org/10.5194/BG-2023-146

Diffenbaugh, N. S., Barnes, E. A., & Keys, P. W. (2023). Probability of continued local-scale warming and extreme events during and after decarbonization. *Environmental Research: Climate*, *2*(2), 021003. https://doi.org/10.1088/2752-5295/ACCF2F

Dittus, A. J., Collins, M., Sutton, R., & Hawkins, E. (2024). Reversal of projected European summer precipitation decline in a stabilizing climate. *Geophysical Research Letters*, *51*(6), e2023GL107448. https://doi.org/10.1029/2023GL107448

Eyring, V., Bony, S., Meehl, G. A., Senior, C. A., Stevens, B., Stouffer, R. J., & Taylor, K. E. (2016). Overview of the coupled model intercomparison project phase 6 (CMIP6) experimental design and organization. *Geoscientific Model Development*, *9*(5), 1937–1958. https://doi.org/10.5194/gmd-9-1937-2016

Eyring, V., Gillett, N. P., Achuta Rao, K. M., Barimalala, R., Barreiro Parrillo, M., Bellouin, N., et al. (2021). Human influence on the climate system. In *Climate change 2021–The physical science basis* (pp. 423–552). Cambridge University Press. https://doi.org/10.1017/9781009157896.005

Forster, P. M., Smith, C., Walsh, T., Lamb, W. F., Lamboll, R., Cassou, C., et al. (2025). Indicators of global climate change 2024: Annual update of key indicators of the state of the climate system and human influence. *Earth System Science Data*, *17*(6), 2641–2680. https://doi.org/10.5194/ESSD-2025-250

Grose, M. R., & King, A. D. (2023). The circulation and rainfall response in the southern hemisphere extra-tropics to climate stabilisation. *Weather and Climate Extremes*, *41*, 100577. https://doi.org/10.1016/J.WACE.2023.100577

Hausfather, Z. (2025). An assessment of current policy scenarios over the 21st century and the reduced plausibility of high-emissions pathways. *Dialogues on Climate Change*, *2*(1), 26–32. https://doi.org/10.1177/29768659241304854

Hawkins, E., Frame, D. J., Harrington, L., Joshi, M. M., King, A. D., Rojas, M., & Sutton, R. (2020). Observed emergence of the climate change signal: From the familiar to the unknown. *Geophysical Research Letters*, *47*(6), e2019GL086259. https://doi.org/10.1029/2019GL086259

Hawkins, E., & Sutton, R. (2009). The potential to narrow uncertainty in regional climate predictions. *Bulletin of the American Meteorological Society*, *90*(8), 1095–1107. https://doi.org/10.1175/2009BAMS2607.1

Huard, D., Fyke, J., Capellán-Pérez, I., Matthews, H. D., & Partanen, A. I. (2022). Estimating the likelihood of GHG concentration scenarios from probabilistic integrated assessment model simulations. *Earth's Future*, *10*(10), e2022EF002715. https://doi.org/10.1029/2022EF002715

Iturbide, M., Gutiérrez, J. M., Alves, L. M., Bedia, J., Cerezo-Mota, R., Cimadevilla, E., et al. (2020). An update of IPCC climate reference regions for subcontinental analysis of climate model data: Definition and aggregated datasets. *Earth System Science Data*, *12*(4), 2959–2970. https://doi.org/10.5194/ESSD-12-2959-2020

Jackson, L. C., Schaller, N., Smith, R. S., Palmer, M. D., & Vellinga, M. (2014). Response of the Atlantic meridional overturning circulation to a reversal of greenhouse gas increases. *Climate Dynamics*, *42*(11–12), 3323–3336. https://doi.org/10.1007/S00382-013-1842-5/TABLES/2

Jones, C. D., Frölicher, T. L., Koven, C., MacDougall, A. H., Matthews, H. D., Zickfeld, K., et al. (2019). The zero emissions commitment model intercomparison project (ZECMIP) contribution to C4MIP: Quantifying committed climate changes following zero carbon emissions. *Geoscientific Model Development*, *12*(10), 4375–4385. https://doi.org/10.5194/gmd-12-4375-2019

King, A. (2024). ACCESS-ESM-1.5 net-zero emissions 1000-year long simulations: Seasonal temperature and precipitation gridded data with area-average timeseries of temperature, precipitation and sea ice data. *Zenodo*. https://doi.org/10.5281/zenodo.13168507

King, A. (2025). Scripts and additional data in support of detectability of post-net zero climate changes and the effects of delay in emissions cessation. *Zenodo*. https://doi.org/10.5281/zenodo.15875474

King, A. D., Donat, M. G., Fischer, E. M., Hawkins, E., Alexander, L. V., Karoly, D. J., et al. (2015). The timing of anthropogenic emergence in simulated climate extremes. *Environmental Research Letters*, *10*(9), 094015. https://doi.org/10.1088/1748-9326/10/9/094015

King, A. D., Jones, C. D., Ziehn, T., Perkins-Kirkpatrick, S., Hirsch, A. L., & Cassidy, L. (2025). Enhancing communication of climate changes under net zero emissions. *Communications Earth & Environment*, *6*(1), 526. https://doi.org/10.1038/s43247-025-02472-1

King, A. D., Lane, T. P., Henley, B. J., & Brown, J. R. (2020). Global and regional impacts differ between transient and equilibrium warmer worlds. *Nature Climate Change*, *10*(1), 42–47. https://doi.org/10.1038/s41558-019-0658-7

King, A. D., Peel, J., Ziehn, T., Bowen, K. J., McClelland, H. L. O., McMichael, C., et al. (2022). Preparing for a post-net-zero world. *Nature Climate Change*, *12*(9), 775–777. https://doi.org/10.1038/s41558-022-01446-x

King, A. D., Sniderman, J. M. K., Dittus, A. J., Brown, J. R., Hawkins, E., & Ziehn, T. (2021). Studying climate stabilization at Paris agreement levels. *Nature Climate Change*, *11*(12), 1010–1013. https://doi.org/10.1038/s41558-021-01225-0

King, A. D., Ziehn, T., Chamberlain, M., Borowiak, A. R., Brown, J. R., Cassidy, L., et al. (2024). Exploring climate stabilisation at different global warming levels in ACCESS-ESM-1.5. *Earth System Dynamics*, *15*(5), 1353–1383. https://doi.org/10.5194/ESD-15-1353-2024

Lacroix, F., Burger, F. A., Silvy, Y., Schleussner, C.-F., & Frölicher, T. L. (2024). Persistently elevated high-latitude ocean temperatures and global sea level following temporary temperature overshoots. *Earth's Future*, *12*(10), e2024EF004862. https://doi.org/10.1029/2024EF004862

Lehner, F., & Deser, C. (2023). Origin, importance, and predictive limits of internal climate variability. *Environmental Research: Climate*, *2*(2), 023001. https://doi.org/10.1088/2752-5295/ACCF30

Long, S.-M., Xie, S. P., Du, Y., Liu, Q., Zheng, X. T., Huang, G., et al. (2020). Effects of ocean slow response under low warming targets. *Journal of Climate*, *33*(2), 477–496. https://doi.org/10.1175/JCLI-D-19-0213.1

MacDougall, A. H., Frölicher, T. L., Jones, C. D., Rogelj, J., DamonMatthews, H., Zickfeld, K., et al. (2020). Is there warming in the pipeline? A multi-model analysis of the zero emissions commitment from CO2. *Biogeosciences*, *17*(11), 2987–3016. https://doi.org/10.5194/BG-17-2987-2020

MacDougall, A. H., Mallett, J., Hohn, D., & Mengis, N. (2022). Substantial regional climate change expected following cessation of CO2 emissions. *Environmental Research Letters*, *17*(11), 114046. https://doi.org/10.1088/1748-9326/AC9F59

MacDougall, A. H., Rogelj, J., Jones, C. D., Liddicoat, S. K., & Grassi, G. (2024). Detecting climate milestones on the path to climate stabilization. *Environmental Research Letters*, *19*(7), 074065. https://doi.org/10.1088/1748-9326/AD5AB1

Mahlstein, I., Hegerl, G., & Solomon, S. (2012). Emerging local warming signals in observational data. *Geophysical Research Letters*, *39*(21). https://doi.org/10.1029/2012GL053952

Mahlstein, I., Knutti, R., Solomon, S., & Portmann, R. W. (2011). Early onset of significant local warming in low latitude countries. *Environmental Research Letters*, *6*(3), 034009. https://doi.org/10.1088/1748-9326/6/3/034009

Manabe, S., Stouffer, R. J., Spelman, M. J., & Bryan, K. (1991). Transient responses of a coupled ocean–atmosphere model to gradual changes of atmospheric CO2. Part I. Annual mean response. *Journal of Climate*, *4*(8), 785–818. https://doi.org/10.1175/1520-0442(1991)004<0785:TROACO>2.0.CO;2

Marotzke, J. (2019). Quantifying the irreducible uncertainty in near-term climate projections. *Wiley Interdisciplinary Reviews: Climate Change*, *10*(1), e563. https://doi.org/10.1002/WCC.563

McKenna, C. M., Maycock, A. C., Forster, P. M., Smith, C. J., & Tokarska, K. B. (2020). Stringent mitigation substantially reduces risk of unprecedented near-term warming rates. *Nature Climate Change*, *11*(2), 126–131. https://doi.org/10.1038/s41558-020-00957-9

Mengel, M., Nauels, A., Rogelj, J., & Schleussner, C.-F. (2018). Committed sea-level rise under the Paris agreement and the legacy of delayed mitigation action. *Nature Communications*, *9*(1), 601. https://doi.org/10.1038/s41467-018-02985-8

Min, S.-K., Zhang, X., Zwiers, F. W., & Hegerl, G. C. (2011). Human contribution to more-intense precipitation extremes. *Nature*, *470*(7334), 378–381. https://doi.org/10.1038/nature09763

Min, S.-K., Zhang, X., Zwiers, F. W., Shiogama, H., Tung, Y.-S., & Wehner, M. (2013). Multimodel detection and attribution of extreme temperature changes. *Journal of Climate*, *26*(19), 7430–7451. https://doi.org/10.1175/JCLI-D-12-00551.1

O'Neill, B. C., Tebaldi, C., Van Vuuren, D. P., Eyring, V., Friedlingstein, P., Hurtt, G., et al. (2016). The scenario model intercomparison project (ScenarioMIP) for CMIP6. *Geoscientific Model Development*, *9*(9), 3461–3482. https://doi.org/10.5194/gmd-9-3461-2016

Paik, S., Min, S. K., Zhang, X., Donat, M. G., King, A. D., & Sun, Q. (2020). Determining the anthropogenic greenhouse gas contribution to the observed intensification of extreme precipitation. *Geophysical Research Letters*, *47*(12), e2019GL086875. https://doi.org/10.1029/2019GL086875

Pfleiderer, P., Schleussner, C.-F., & Sillmann, J. (2024). Limited reversal of regional climate signals in overshoot scenarios. *Environmental Research: Climate*, *3*(1), 015005. https://doi.org/10.1088/2752-5295/AD1C45

Roldán-Gómez, P. J., De Luca, P., Bernardello, R., & Donat, M. G. (2025). Regional irreversibility of mean and extreme surface air temperature and precipitation in CMIP6 overshoot scenarios associated with interhemispheric temperature asymmetries. *Earth System Dynamics*, *16*(1), 1–27. https://doi.org/10.5194/ESD-16-1-2025

Romanzini-Bezerra, G., & Maycock, A. C. (2024). Projected rapid response of stratospheric temperature to stringent climate mitigation. *Nature Communications*, *15*(1), 1–6. https://doi.org/10.1038/s41467-024-50648-8

Sarofim, M. C., Smith, C. J., Malek, P., McDuffie, E. E., Hartin, C. A., Lay, C. R., & McGrath, S. (2024). High radiative forcing climate scenario relevance analyzed with a ten-million-member ensemble. *Nature Communications*, *15*(1), 1–10. https://doi.org/10.1038/S41467-024-52437-9

Schleussner, C.-F., Ganti, G., Lejeune, Q., Zhu, B., Pfleiderer, P., Prütz, R., et al. (2024). Overconfidence in climate overshoot. *Nature*, *634*(8033), 366–373. https://doi.org/10.1038/s41586-024-08020-9

Schwinger, J., Asaadi, A., Goris, N., & Lee, H. (2022). Possibility for strong northern hemisphere high-latitude cooling under negative emissions. *Nature Communications*, *13*(1), 1–9. https://doi.org/10.1038/S41467-022-28573-5

Schwinger, J., Asaadi, A., Steinert, N. J., & Lee, H. (2022). Emit now, mitigate later? Earth system reversibility under overshoots of different magnitudes and durations. *Earth System Dynamics*, *13*(4), 1641–1665. https://doi.org/10.5194/ESD-13-1641-2022

Seneviratne, S. I., Zhang, X., Adnan, M., Badi, W., Dereczynski, C., Di Luca, A., et al. (2021). Weather and climate extreme events in a changing climate. In V. Masson-Delmotte, P. Zhai, A. Pirani, S. L. Connors, C. Pean, S. Berger, et al. (Eds.), *Climate change 2021: The physical science basis. Contribution of working group I to the sixth assessment report of the intergovernmental panel on climate change* (pp. 1513–1766). Cambridge University Press. https://doi.org/10.1017/9781009157896.013

Sniderman, J. M. K., Brown, J. R., Woodhead, J. D., King, A. D., Gillett, N. P., Tokarska, K. B., et al. (2019). Southern hemisphere subtropical drying as a transient response to warming. *Nature Climate Change*, *9*(3), 232–236. https://doi.org/10.1038/s41558-019-0397-9

Sowers, T., Alley, R. B., & Jubenville, J. (2003). Ice core records of atmospheric N2O covering the last 106,000 years. *Science*, *301*(5635), 945–948. https://doi.org/10.1126/science.1085293

United Nations Environment Programme. (2024). Emissions gap report 2024. *United Nations Environment Programme*. https://doi.org/10.59117/20.500.11822/46404

van Vuuren, D., O'Neill, B., Tebaldi, C., Chini, L., Friedlingstein, P., Hasegawa, T., et al. (2025). The scenario model intercomparison project for CMIP7 (ScenarioMIP-CMIP7). *EGUsphere*, *30*, 1–38. https://doi.org/10.5194/EGUSPHERE-2024-3765

Walton, J., & Huntingford, C. (2024). Little evidence of hysteresis in regional precipitation, when indexed by global temperature rise and fall in an overshoot climate simulation. *Environmental Research Letters*, *19*(8), 084028. https://doi.org/10.1088/1748-9326/AD60DE

Weijer, W., Cheng, W., Garuba, O. A., Hu, A., & Nadiga, B. T. (2020). CMIP6 models predict significant 21st century decline of the Atlantic meridional overturning circulation. *Geophysical Research Letters*, *47*(12), e2019GL086075. https://doi.org/10.1029/2019GL086075

Wilks, D. S. (2011). *Statistical methods in the atmospheric sciences*. Elsevier/Academic Press.

Zeder, J., Sippel, S., Pasche, O. C., Engelke, S., & Fischer, E. M. (2023). The effect of a short observational record on the statistics of temperature extremes. *Geophysical Research Letters*, *50*(16), e2023GL104090. https://doi.org/10.1029/2023GL104090

Zhang, X., Wan, H., Zwiers, F. W., Hegerl, G. C., & Min, S. K. (2013). Attributing intensification of precipitation extremes to human influence. *Geophysical Research Letters*, *40*(19), 5252–5257. https://doi.org/10.1002/GRL.51010

Zhang, Z., Poulter, B., Melton, J. R., Riley, W. J., Allen, G. H., Beerling, D. J., et al. (2025). Ensemble estimates of global wetland methane emissions over 2000-2020. *Biogeosciences*, *22*(1), 305–321. https://doi.org/10.5194/BG-22-305-2025

Zhang, Z., Zimmermann, N. E., Stenke, A., Li, X., Hodson, E. L., Zhu, G., et al. (2017). Emerging role of wetland methane emissions in driving 21st century climate change. *Proceedings of the National Academy of Sciences of the United States of America*, *114*(36), 9647–9652. https://doi.org/10.1073/pnas.1618765114

Ziehn, T., Chamberlain, M., Lenton, A., Law, R., Bodman, R., Dix, M., et al. (2019a). CSIRO ACCESS-ESM1.5 model output prepared for CMIP6 CMIP'. https://doi.org/10.22033/ESGF/CMIP6.2288

Ziehn, T., Chamberlain, M., Lenton, A., Law, R., Bodman, R., Dix, M., et al. (2019b). CSIRO ACCESS-ESM1.5 model output prepared for CMIP6 ScenarioMIP'. https://doi.org/10.22033/ESGF/CMIP6.2291